OPEN ACCESS Freely available online

Research Article

Vol. 1, Issue 1, January-December 2026

Journal of Mathematics, Physics and Mechanics

Green Synthesis of Co_3O_4 Nanoparticles Using *Moringa oleifera* Leaf Extract: Structural and Optical Study from a Materials Physics Perspective

Priyanshi Varshney[1], Hamza Mustapha Umar[1,2*], Akhilesh Dwivedi[1], Mohammad Aamir[3]

[1]*Department of Physics, Mewar University, Chittorgarh, Rajasthan, India*

[2]*Department of Physics, Northwest University, Kano, Nigeria*

[3]*Center for Advanced Materials and Devices, BML Munjal University, Gurugram, India*

***Correspondence to:** Hamza Mustapha Umar[1,2], [1]Department of Physics, Mewar University, Chittorgarh, Rajasthan, India; [2]Department of Physics, Northwest University, Kano, Nigeria, E-mail: hamzamustaphaumar@gmail.com

Received: October 04, 2026; **Manuscript No:** JMPM-26-5292; **Editor Assigned:** October 07, 2026; **PreQc No:** JMPM-26-5292 (PQ); **Reviewed:** October 22, 2026; **Revised:** October 23, 2026; **Accepted:** October 26, 2026; **Published:** November 20, 2026

Citation: Varshney P, Umar HM, Dwivedi A, Aamir M (2026). Green Synthesis of Co_3O_4 Nanoparticles Using *Moringa oleifera* Leaf Extract: Structural and Optical Study from a Materials Physics Perspective. J. Math. Phys. Mech. Vol.1 Iss.1, November (2026), pp:395-403.

Copyright: © 2026 Priyanshi Varshney, Hamza Mustapha Umar, Akhilesh Dwivedi, Mohammad Aamir. This is an open-access article distributed under the terms of the Creative Commons Attribution License, which permits unrestricted use, distribution, and reproduction in any medium, provided the original author and source are credited.

ABSTRACT

In the present study, Co_3O_4 nanoparticles were synthesized by Moringa oleifera leaf extract and characterized by XRD, FTIR, SEM, EDX, and UV-Visible spectroscopy. Cobalt (II) chloride was used as the precursor with an extract-to-salt ratio of 3:1, then precipitated at a pH of 10, dried at 100 °C, and calcined at 450 °C for 3 h. XRD confirmed the formation of cubic spinel Co_3O_4 corresponding to JCPDS 42-1467 with a mean crystallite size of 21.6 ± 5.1 nm. FTIR bands at 655, 539, 472, and 418 cm^{-1} were assigned to Co–O vibrations of the spinel structure, with other bands due to surface species from the plants. SEM revealed predominantly pseudo-cubic and polyhedral particles, with micrometer-scale aggregation and some rod-like features. EDX showed the main elements, cobalt and oxygen. UV-visible analysis showed strong absorption around 245 nm, and Tauc analysis gave a direct optical band gap of 3.31 eV. The overall results confirm the formation of crystalline Co_3O_4 with different structural, morphological, and optical properties via a Moringa oleifera-mediated route, which paves the way for further investigation in photocatalytic, sensing, and electrochemical applications.

Keywords: Co_3O_4 Nanoparticles; Moringa oleifera; Green Synthesis; Spinel Oxide; XRD; FTIR; SEM; EDX; UV–Visible Spectroscopy; Optical Band Gap

INTRODUCTION

Cobalt oxide is a very interesting member of the transition-metal oxide family. Co_3O_4 has a cubic spinel structure, in which Co^{2+} and Co^{3+} ions reside in tetrahedral and octahedral sites, respectively. This mixed-valence configuration endows the material with unique electronic, catalytic, and electrochemical properties and has sparked research in gas sensing, photocatalysis, energy storage, and electrocatalysis. Recent reviews also highlight that the nanoscale structure of Co_3O_4 is very sensitive to synthesis conditions, with morphology, defect chemistry, surface area, and crystallite size impacting the response measured [1–5].

The biogenic synthesis of Co_3O_4 has been rapidly expanded. Recent studies have reported plant sources such as Moringa oleifera, Muntingia calabura, lemon, Aloe barbadensis, Lawsonia inermis, spent coffee, and other botanical materials. The results of these studies show that plant-based systems can produce crystalline Co_3O_4 with different sizes, shapes, and optical properties. Importantly, the variation between studies also explains why synthesis conditions and characterization should be reported simultaneously, rather than treating "green synthesis" as a single standardized method [6–16].

Moringa oleifera is of particular relevance because its leaves contain a wide range of phenolic and flavonoid compounds, and the plant is already widely explored as a source of bioactive molecules for nanomaterial synthesis. Green synthesis based on Moringa has been applied to several metal and metal-oxide systems, and recent work has focused on cobalt oxide derived from Moringa seed extract. Nevertheless, the leaf extract route offers a different phytochemical environment than the seed-based synthesis and needs direct structural and optical characterization [8, 17–19].

The present work focuses only on Co_3O_4 derived from Moringa oleifera leaf extract. The goal is not to state an application performance, which was not experimentally assessed, but to find a consistent relationship between phase formation, crystallite size, vibrational fingerprint, morphology, elemental composition, and optical absorption. One synthesis protocol is based on the combination of XRD, FTIR, SEM/EDX, and UV–visible spectroscopy. Special attention is paid to the implications of the measured crystallite size of 21.6 nm and the direct optical band gap of 3.31 eV and their comparison with the recent green-synthesis literature [3–7, 9, 14, 15, 20].

MATERIALS AND METHODS

Materials

Cobalt (II) chloride hexahydrate ($CoCl_2 \cdot 6H_2O$, ≥99%) and sodium hydroxide (NaOH, ≥98%) were used as received. Fresh Moringa oleifera leaves were washed with deionized water, dried at 60°C for 24 h, and powdered to fine powder. The solutions were made up of deionized water of resistivity ~18.2 MΩ cm. The precursor and processing conditions were directly from the experimental procedure in the given manuscript.

Preparation of *Moringa oleifera* Leaf Extract

The dried *Moringa oleifera* leaf powder (20 g) was added to 200 mL deionized water and heated to 80 °C with continuous magnetic stirring for 30 min. The suspension was filtered to give a clear aqueous extract, which was stored at 4°C until use. It is believed that plant-derived hydroxyl- and carbonyl-containing compounds can coordinate metal ions and interact with growing oxide surfaces and thus influence nucleation and particle growth [16–19, 21].

Green Synthesis of Co_3O_4 Nanoparticles

An aqueous solution of 0.1 M $CoCl_2.6H_2O$ was heated at 60°C under stirring. Moringa oleifera extract was added dropwise with a salt solution to an extract volume ratio of 1:3 and stirred at 80°C for 2 h. The reaction mixture was then adjusted to pH 10 with NaOH solution. The precipitate was isolated by centrifugation, washed three times with deionized water and once with ethanol, dried overnight at 100°C, and calcined in air at 450°C for 3 h. The resultant powder was referred to as Co_3O_4. Figure 1 shows the schematic representation of the Moringa oleifera-mediated pathway used for the synthesis of Co_3O_4 nanoparticles. The extract is the plant-derived reaction medium in complexation, nucleation and growth, and then in precipitation, drying, and calcination.

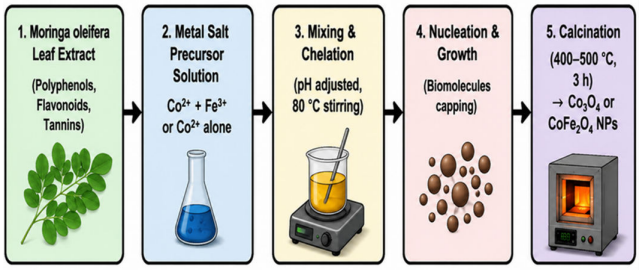


Figure 1: Schematic Representation of the Moringa oleifera-Mediated Route Used to Produce Co_3O_4 Nanoparticles

Characterization

Powder XRD was performed on a PANalytical EMPYREAN diffractometer with Cu Kα radiation (λ = 1.5406 Å) at 45 kV and 40 mA. Diffraction patterns were collected from 20° to 80° (2θ) with a 0.03° step and a counting time of 2 s per step. The crystallite size was estimated by the Scherrer relation $D = K\lambda/\beta \cos\theta$ with K = 0.9. The Fourier transform infrared (FTIR) spectra were recorded in the range of 400–4000 cm^{-1} for the pellet samples with KBr. SEM and EDX were performed on a Hitachi SU3500 at 15.0 kV in secondary-electron mode. UV-visible spectra were measured in the range of 225–800 nm. The direct optical band gap was estimated by the relation $(\alpha h\nu)^2 = A(h\nu - Eg)$.

RESULTS AND DISCUSSION

Crystal Structure and Crystallite Size

The XRD pattern of the prepared material exhibits the typical reflections of cubic spinel Co_3O_4. The peaks observed at 31.39, 36.97, 38.70, 44.98, 55.84, 59.49, 65.38, 69.36, 74.19, and 77.47 correspond to (220), (311), (222), (400), (422), (511), (440), (531), (533), and (622) planes, respectively. The strongest reflection is at 36.97°, corresponding to the (311) plane. The peak sequence is in agreement with the cubic spinel reference pattern JCPDS 42-1467 and is consistent with previously reported Co_3O_4 nanocrystals [1, 2]. The XRD pattern of green synthesized Co_3O_4 nanoparticles is shown in Figure 2. The reflections are in agreement with the cubic spinel Co_3O_4 phase.

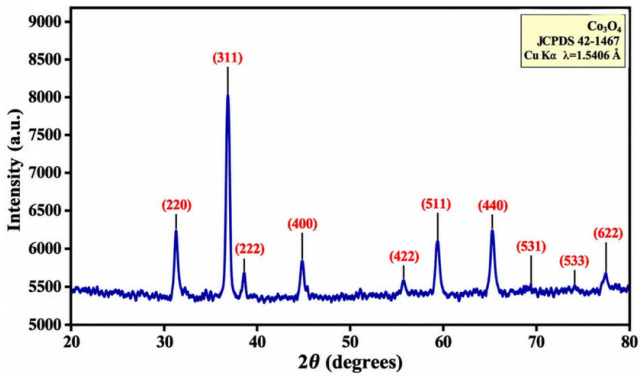


Figure 2: XRD Pattern of Green-Synthesized Co_3O_4 Nanoparticles

The average Scherrer crystallite size was 21.6 ± 5.1 nm. This value places the material well within the nanocrystalline regime and within the broad size range reported for plant-mediated Co_3O_4 systems. The synthesis of Co_3O_4 using moringa seed extract has been reported with a crystallite size of about 18.8 nm. Other plant-mediated routes have resulted in crystallites that are either significantly smaller or larger depending on precursor concentration, extract composition, reaction temperature, and calcination history. The comparison suggests that the present crystallite size is expected for a precipitation–calcination route and should be attributed to the whole processing history, not only to the plant extract [3, 7, 11, 13, 21, 22].

From a solid-state perspective, the diffraction pattern reflects the long-range periodic arrangement of Co and O ions in the spinel lattice. The characteristic (220), (311), (222), (400), (422), (511), (440), (531), (533), and (622) reflections arise from the allowed planes of the cubic structure, while the dominant (311) reflection indicates the preferred intensity contribution of this plane under the present synthesis conditions. The coherent-domain size obtained from peak broadening is related to the finite extent of crystalline order through the Scherrer equation, $D = K\lambda/(\beta \cos \theta)$. Thus, the value of 21.6 nm represents the average dimension over which the lattice remains coherently diffracting and should not be interpreted as the physical diameter of every particle seen by SEM.

The relatively sharp reflections suggest a significant degree of crystallinity after the 450°C calcination step. At the same time, the finite dimensions of crystallites are consistent with the nanoscale peak broadening. Note that the Scherrer crystallite size is not equal to the apparent particle size observed by SEM: a micrometre-scale aggregate may be made up of many nanoscale coherent crystallites. This distinction matters in connecting morphology to optical or catalytic behavior [2, 23, 24].

FTIR Analysis and Surface Chemistry

The FTIR spectrum provides a second structural fingerprint of the synthesized oxide. The main low wavenumber bands are located at about 655, 539, 472, and 418 cm^{-1}. These features are attributed to Co–O lattice vibrations and are consistent with the vibrational response expected for spinel Co_3O_4. The existence of more than one Co-O-related band is due to the different local coordination environments related to cobalt cations in the spinel lattice [1, 25]. Figure 3: FTIR spectrum of the green-synthesized Co_3O_4 nanoparticles showing the characteristic low-wavenumber metal–oxygen bands.

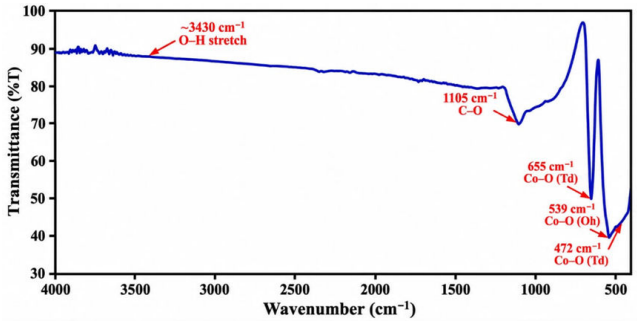


Figure 3: FTIR Spectrum of the Green-Synthesized Co_3O_4 Nanoparticles showing the Characteristic Low-wavenumber Metal–oxygen Bands

Additional absorption features in the higher wavenumber region are consistent with residual organic species associated with the surface from the plant extract. These bands are generally observed after plant-mediated synthesis, and it is because of C-O, C-H, and O-H-containing groups. Presence alone does not demonstrate a particular phytochemical identity. Rather, the spectrum favors the conservative interpretation that some of the functional groups derived from the plant remained bound to the surface of the oxide after washing and calcination [17, 19, 21].

FTIR results confirmed the XRD results. XRD probes long-range crystalline order, and FTIR probes local bonding environments. The agreement between the diffraction pattern of spinel and the low-frequency Co–O bands supports the phase assignment. Similar Co–O fingerprints have been reported for green synthesized Co_3O_4 from different biological sources [4, 6, 7, 10].

Morphology and Elemental Composition

The SEM exhibits a morphology which is more complex than the nominal 21.6 nm crystallite size. The particles are mainly pseudo-cubic to polyhedral, with apparent sizes ranging between ~0.5 and 2 µm, as shown in the micrographs. At higher magnification, finer structural details and a smaller population of rodlike particles can be distinguished. The discrepancy between the apparent SEM aggregate dimensions and the XRD crystallite size suggests that the micrometer-sized objects observed are most likely aggregates of smaller coherent crystallites rather than single 0.5–2 µm crystallites. SEM micrographs of Moringa oleifera-mediated Co_3O_4 at different magnifications are shown in Figure 4. The micrographs show the predominance of pseudo-cubic/polyhedral aggregates at lower magnification and finer features at higher magnification.

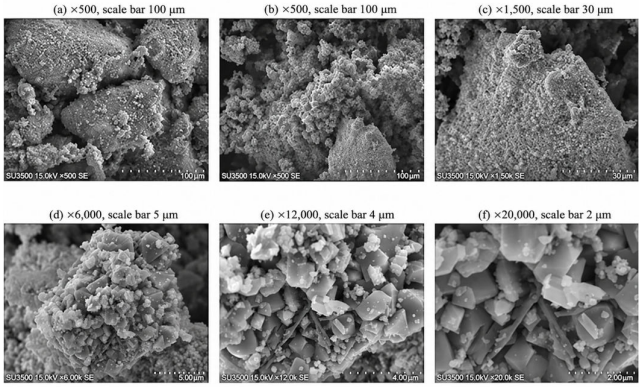


Figure 4: SEM Micrographs of Moringa oleifera-mediated Co_3O_4 at increasing Magnification

The morphology is strongly affected by the precursor concentration, pH, extract-to-metal ratio, drying history, and calcination. Plant-derived molecules can selectively adsorb on growing crystal surfaces and therefore change relative growth rates. However, in the absence of time-resolved growth experiments or surface-specific spectroscopic techniques, the current data do not allow us to identify a unique phytochemical or crystallographic face as the only origin of the observed morphology. A more defendable conclusion is that the plant-mediated synthesis produced a non-uniform aggregate structure with a measurable nanoscale crystallite size [13, 17, 18, 21, 26, 27].

The EDX analysis showed the Co_3O_4 sample was composed of cobalt and oxygen as major elements. The source manuscript also reports a trace Zn signal and carbon for the sample, with the caveat that oxygen can be underestimated in EDX measurements of transition metal oxides. Hence, EDX here is best used as a compositional confirmation and not a definitive stoichiometric measurement. The detection of Co and O, combined with the XRD/FTIR data, suggests the material is cobalt oxide, but the cobalt oxidation states would need to be directly measured by more surface-sensitive techniques such as XPS [1, 28].

UV–Visible Absorption

The UV-visible spectrum shows a strong absorption in the ultraviolet region with the prominent band centered around 245 nm, followed by a change in the spectral profile toward the longer wavelength. The observed ultraviolet response is consistent with electronic transitions of the cobalt–oxygen framework. Co_3O_4 is a mixed-valence semiconductor, and the optical response may include contributions from charge-transfer and d–d transitions related to Co^{2+} and Co^{3+} sites [1, 29, 30]. Figure 5 shows the UV–Visible absorption spectrum of the synthesized Co_3O_4 NPs. The UV absorption is strong at around 245 nm.

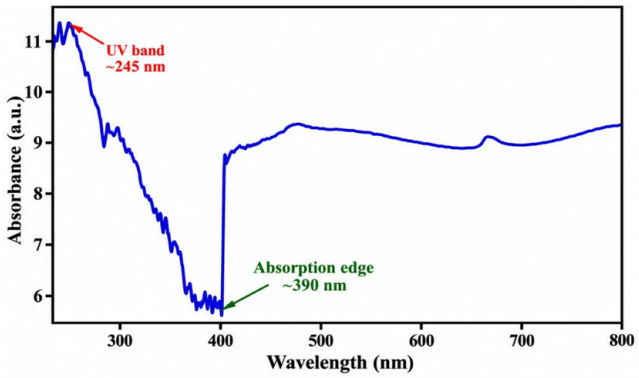


Figure 5: UV–Visible Absorption Spectrum of the Synthesized Co_3O_4 Nanoparticles

Direct Optical Band Gap

The measured spectrum should be distinguished from the optical response of bulk Co_3O_4. Nanoscale crystallinity, surface states, residual surface species, defects, and the method used to determine the absorption coefficient can all influence the apparent absorption edge. Different optical gaps have been found for Co_3O_4 in the reported green-synthesis studies, and thus the result depends on particle size, synthesis route, and analysis model. Hence, the value obtained here is reported as the optical gap of the present sample under the stated measurement and Tauc-analysis conditions and not as a universal band gap for Co_3O_4 [3, 7, 13, 20, 29].

From the linear extrapolation of the appropriate high-energy region, the direct-transition Tauc plot provides an estimated optical band gap of 3.31 eV. This result is higher than many commonly reported values for bulk or defect-rich Co_3O_4 and therefore should be taken with caution. The large apparent gap can arise from nanoscale effects, surface chemistry, the choice of the transition model, the treatment of the baseline, and the way the absorption coefficient is extracted from the measured spectrum [2, 24, 29]. The direct-transition Tauc plot of the synthesized Co_3O_4 nanoparticles is shown in Figure 6, which gives an estimated optical band gap of 3.31 eV.

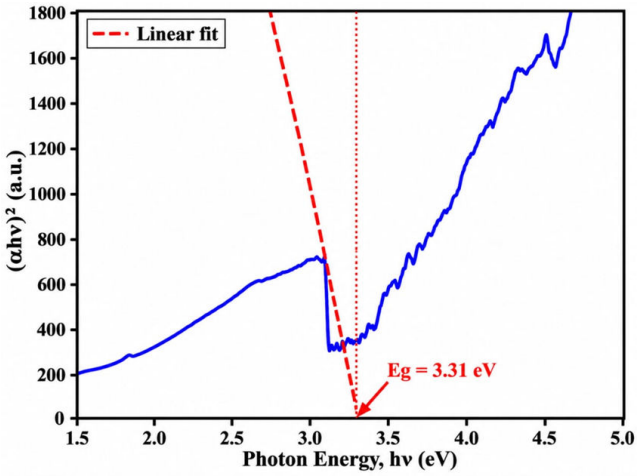


Figure 6: Direct-transition Tauc plot for the Synthesized Co_3O_4 Nanoparticles

The 21.6 nm crystallite size provides a physically reasonable nanoscale context for discussing size-dependent optical behaviour, but the present dataset does not independently establish quantum confinement as the sole origin of the 3.31 eV value. The more rigorous interpretation is that the optical gap reflects the combined influence of crystallite size, defects, surface chemistry and the electronic structure of the prepared sample. This distinction is important because recent green-synthesis studies have reported Co_3O_4 band gaps ranging from approximately 2 to above 3 eV depending on synthesis and characterization conditions [3, 4, 7, 13, 29, 31].

The optical response can also be considered in terms of the electronic structure of the spinel lattice. In Co_3O_4, the coexistence of Co^{2+} and Co^{3+} ions in different coordination environments produces several possible electronic transitions involving cobalt 3d states and the O 2p-derived states. Consequently, the absorption edge is sensitive not only to the average crystallite size but also to defects, surface states, local coordination and residual surface species. The measured 3.31 eV value therefore describes the optical transition obtained from the present sample using the direct-transition Tauc model. Within this framework, the structural and optical measurements are physically connected: the nanocrystalline domains provide a large fraction of surface and interfacial regions, while the crystallographic order and local Co–O bonding determine the electronic states through which optical absorption occurs.

Structure–Property Relationship

The characterization results form a consistent structure–property picture. XRD identifies crystalline cubic spinel Co_3O_4 and gives a mean coherent-domain size of 21.6 ± 5.1 nm. FTIR detects the corresponding Co–O vibrational fingerprint associated with the local coordination of cobalt within the spinel lattice. SEM shows that these nanocrystalline domains occur within larger aggregates, while EDX confirms cobalt and oxygen as the principal detected constituents. UV–Visible spectroscopy demonstrates strong ultraviolet absorption, and the Tauc analysis yields a direct optical gap of 3.31 eV. These observations are physically complementary: long-range crystal order controls the diffraction response, local Co–O bonding determines the vibrational modes, and the electronic structure of the mixed-valence oxide governs the optical transitions. The aggregation observed by SEM does not contradict the nanocrystalline XRD result because each larger aggregate can contain many coherently diffracting domains.

The synthesis route gives a possible link between the plant extract and the obtained structure. During extraction, water-soluble phytochemicals are transferred into the reaction medium. After the addition of the cobalt salt, functional groups able to coordinate can interact with Co^{2+} species. Further increase in alkalinity causes precipitation; drying and calcination convert the precursor to the crystalline oxide. The calcination temperature influences the conversion to the final oxide phase, and the presence of surface-

attached organic matter may also influence the early stages of nucleation and growth. This mechanism is in agreement with the general literature on plant-mediated formation of nanomaterials [17–19, 21, 26].

The data also emphasize the necessity of describing a green synthesis with all the parameters of the whole process. The resulting material cannot be defined by the plant extract alone because phase purity, crystallite size, surface residue, and morphology are influenced by extract concentration, precursor concentration, pH, mixing time, drying temperature, and calcination schedule. Recent comparative studies on plant-mediated Co_3O_4 synthesis generally conclude the same: green chemistry provides a useful synthetic platform, but the need for strict control of materials-processing variables remains [3, 8, 14, 15, 20].

Comparison with Recent Literature

In Table 1, the current material is compared with some studies on Co_3O_4 through biological or low-impact synthesis routes. Direct numerical comparison should be made with caution since reported values are obtained with different precursors, extracts, calcination temperatures, particle size definitions and optical models. Hence, the table is meant to provide context rather than rank one synthesis route as universally superior.

Study	Biogenic source	Crystallite/particle size	Optical/structural result	DOI
Present study	Moringa oleifera leaf	21.6 ± 5.1 nm	Co_3O_4 spinel; Eg = 3.31 eV	Source manuscript
Bharathi et al. (2023)	Moringa oleifera seed	~18.8 nm	Cubic Co_3O_4; Eg ≈ 3.20 eV	10.1007/s10854-022-09506-w
Rajan et al. (2021)	Sargassum tenerrimum	Reported Co_3O_4 NPs	Photocatalytic/antibacterial study	10.1007/s13204-021-01774-6
Ogunyemi et al. (2023)	Hibiscus rosa-sinensis	~34.9 nm	Biogenic Co_3O_4 with biological activity	10.1016/j.ecoenv.2023.114935
Raimundo et al. (2023)	Plantago ovata	Co_3O_4 NPs	Green electrocatalyst for OER	10.1016/j.jelechem.2023.117218
Poonguzhali et al. (2023)	Lemon extract	16.2–26.9 nm	Spinel Co_3O_4; LPG sensing	10.1016/j.snb.2022.133036
Anuradha & Raji (2024)	Beta vulgaris	34.9 nm	Optical/dielectric Co_3O_4	10.1007/s00339-024-07830-y
Drummer et al. (2024)	Spent coffee	Co_3O_4 NPs	Photocatalytic/catalytic dye degradation	10.1016/j.nxnano.2024.100069
Sarvalkar et al. (2024)	Aloe barbadensis	Biogenic Co_3O_4	Photocatalytic/biological studies	10.1016/j.rineng.2024.102094
Kader (2024)	Garlic extract	Co_3O_4 NPs	Green-light catalytic oxidation	10.1016/j.mtsust.2024.100997

Table 1: Comparison of the Study with the Previous Literature

The current crystallite size is comparable to that reported for Co_3O_4 derived from Moringa seed, but the botanical material is different. The scientific relevance of the difference between leaf and seed extracts is that their metabolite profiles are not the same. The present sample also shows a larger apparent direct optical gap than a number of other reported Co_3O_4 systems. This difference does not evidence superior performance but rather indicates that the optical response is synthesis-dependent and needs further validation by diffuse-reflectance spectroscopy, photoluminescence, and surface-sensitive measurements [3, 7, 8, 11, 13].

Potential Functional Relevance and Study Limitations

Co_3O_4 has been studied as a semiconductor, gas sensor material, catalyst, and electrochemical electrode. Recent studies have also shown green-synthesized Co_3O_4 in photocatalytic dye degradation, oxygen evolution, and gas sensing. The present structural and optical results therefore justify the selection of this material for further functional experiments. However, this study did not measure any photocatalytic rate constant, gas-sensor response, electrochemical capacitance, or antimicrobial inhibition zone. Those quantities should not be derived from the characterization data only [4, 9, 11, 16, 32–34].

The main limitations are thus experimental in scope, not evidence of a failed synthesis. XPS would strengthen the study to resolve Co2+/Co3+ surface chemistry, Raman spectroscopy to provide an additional spinel fingerprint, BET analysis to quantify specific surface area, photoluminescence to probe carrier recombination, and electrochemical or photocatalytic measurements to connect structure directly with performance. Such additions make it possible to convert the current characterization dataset into a more comprehensive structure-function study [1, 5, 9].

Future Scope

The present results provide a useful materials baseline, but several experiments are needed before quantitative application claims can be made. First, the surface ratio of Co^{2+}/Co^{3+} and the chemical state of oxygen should be determined by XPS. This would complement the bulk-sensitive XRD and bonding information from FTIR and help determine if surface defects or mixed-valence distributions contribute to the measured optical response [1, 28].

Secondly, the optical properties should be augmented with diffuse reflectance UV–Vis spectroscopy, photoluminescence, and, if possible, valence band measurements. Such data would be useful to test the robustness of the 3.31 eV Tauc value to the measurement geometry and transition model assumptions. It has been found that the optical gap for green Co_3O_4 systems can be strongly dependent on the synthesis conditions, defect states, and surface modification [3, 7, 15, 16, 20, 29].

Third, the material should be tested in a controlled photocatalytic experiment with fixed pollutant concentration, catalyst dosage, pH, light wavelength and intensity, and sampling interval. Kinetic constants should be calculated instead of only reporting the percentage of degradation. Recent studies on Co_3O_4 demonstrate the significance of these parameters when comparing the photocatalytic performance between different green synthesis routes [4, 9, 10, 16].

Fourth, the nanoscale Co_3O_4 should be electrochemically characterized as a supercapacitor or oxygen-evolution material. Co_3O_4 is attractive due to the reversible cobalt redox chemistry, but the performance depends strongly on the electrode architecture, conductivity, porosity, and mass loading. Recent reviews and studies in experiments show that nanosheet arrays, porous structures, and carbon-supported architectures can greatly change electrochemical behavior [5, 30, 34–37].

Finally, a note on reproducibility and scale-up is warranted. Future work should involve comparison of independent batches of Moringa leaf extract, quantification of major phytochemical groups, and testing of the effects of extract concentration and calcination temperature on crystallite size and morphology. A systematic design-of-experiments approach would assist in discriminating the effect of botanical chemistry from that of conventional processing variables. This is particularly important if the synthesis changes from the production of powders in the laboratory to the production of reproducible functional devices or environmental treatment systems [3, 14, 15, 17, 18, 38,39].

CONCLUSION

Co_3O_4 nanoparticles have been successfully synthesized through an aqueous precipitation and calcination route mediated by Moringa oleifera leaf extract. XRD confirmed the cubic spinel Co_3O_4 phase and provided a mean crystallite size of 21.6 ± 5.1 nm. FTIR exhibited characteristic Co-O vibrational bands at 655, 539, 472, and 418 cm^{-1}. SEM exhibited mainly pseudo-cubic/polyhedral aggregates with finer nanoscale features. EDX confirmed the presence of cobalt and oxygen as the main detected elements. UV–Visible spectroscopy revealed a significant absorption around 245 nm and the direct transition. The Tauc analysis gave an apparent optical band gap of 3.31 eV. The combined dataset indicates that Moringa oleifera extract can provide a viable biogenic route to crystalline Co_3O_4 under the processing conditions reported. More importantly, the results establish a clear distinction between what has been measured and what is yet to be tested. The current material is well suited for subsequent photocatalytic, sensing, and electrochemical investigations; however, the quantitative application performance has to be experimentally established. The next level of structure–property evidence would be future XPS, Raman, BET, photoluminescence, and application-specific measurements.

AUTHOR CONTRIBUTIONS

Priyanshi Varshney: Conceptualization, methodology, investigation, formal analysis, data curation and original drafting.

Hamza Mustapha Umar: methodology, formal analysis, software, investigation, review and editing.

Akhilesh Dwivedi: supervision, validation, resources, review and editing.

Mohammad Aamir: Software, resources and formal analysis.

ACKNOWLEDGEMENTS

The authors acknowledge the Department of Physics, Mewar University, Chittorgarh, India, for academic support and access to facilities, and the Center for Advanced Materials and Devices (CAMD), BML Munjal University, Gurugram, India, for characterization support and technical assistance.

CONFLICT OF INTEREST

The authors declare no conflict of interest.

DATA AVAILABILITY

The raw XRD, FTIR, SEM, EDX and UV–Visible datasets supporting the reported results are available from the corresponding author upon reasonable request.

REFERENCES

1. Kim JG, Pugmire DL, Bhattacharyya D, Langell MA. Analysis of the Co3O4 spinel surface with Auger and X-ray photoelectron spectroscopy. Appl Surf Sci. 2000;165(1):70-84.
2. Wang Z, Chen X, Mo M, Zhu X, Yu W, Qian Y. Synthesis of Co3O4 nanocrystals in different morphologies from a new method. J Colloid Interface Sci. 2004;276(2):451-454.
3. Supin KK, Vasundhara M. Lepidagathis ananthapuramensis leaf extract stabilized Co3O4 nanoparticles and its structural, optical and magnetic properties. J Supercond Nov Magn. 2024;37:1743-1753.
4. Prabakaran E, Pillay K. Synthesis of fluorescent N-CDs/ZnO nanocomposites with Moringa oleifera as a carbon source for the photodegradation of methylene blue dye under UV and visible light. RSC Adv. 2021;11(36):22539-22563.
5. Desai RS, Jadhav VS, Patil PS, Dalavi DS. Recent advances in hydrothermally and solvothermally grown Co3O4 nanostructures for electrochemical energy storage applications: a brief review. Mater Adv. 2024;5(3):920-960.
6. Rajan A, Shanmugam S, Venugopal V, Narayanan V. Biogenic synthesis of cobalt oxide nanoparticles using Sargassum tenerrimum aqueous extract and their photocatalytic and antibacterial activities. Appl Nanosci. 2021;11:1747-1758.
7. Bharathi G, Nataraj D, Bhuvaneswari S, Ramadas M, Premkumar T, Thangadurai TD, et al. Evaluation of the physicochemical characteristics and photocatalytic activity of cobalt oxide nanoparticles derived from Moringa seed extract. J Mater Sci Mater Electron. 2023;34:89.
8. Abd Rani N, Ahmad AL, Jawad ZA, Low SC, Zein SH. Moringa oleifera leaf-based zinc oxide nanoparticles: Green synthesis, characterization, and their antibacterial investigations. Inorg Chem Commun. 2023;157:111393.
9. Drummer S, Mkhari O, Chowdhury M. Green synthesis of Co3O4 nanoparticles using spent coffee: application in catalytic and photocatalytic dye degradation. Next Nanotechnol. 2024;6:100069.
10. Sarvalkar PD, Jamadar AS, Kakade SS, Magdum AB, Pawar PK, Yadav JB, et al. Biogenic synthesis of Co3O4 nanoparticles from Aloe barbadensis extract: antioxidant and antimicrobial activities, and photocatalytic degradation of azo dyes. Results Eng. 2024;22:102094.
11. Poonguzhali RV, Kumar ER, Srinivas C, Alshareef M, Aljohani MM, Keshk AA, et al. Natural lemon extract assisted green synthesis of spinel Co3O4 nanoparticles for LPG gas sensor application. Sens Actuators B Chem. 2023;377:133036.
12. Ogunyemi SO, Xu X, Xu L, Abdallah Y, Rizwan M, Lv L, et al. Cobalt oxide nanoparticles: An effective growth promoter of Arabidopsis plants and nano-pesticide against bacterial leaf blight pathogen in rice. Ecotoxicol Environ Saf. 2023;257:114935.
13. Anuradha CT, Raji P. Hydrothermal biosynthetic nanoarchitectonics of cobalt oxide nanoparticles using Beta vulgaris extract: analysis of structural, optical, and insulating properties. Appl Phys A. 2024;130:690.
14. Tesfaye GA, Lemma YS, Mekonon FS, Adera KM, Bekele ET. Green synthesis of ZnO and Co3O4 nanoparticles using giant Calotrope leaf extract for antimicrobial applications. ChemistrySelect. 2024;9:e202403757.
15. Imtiyaz A, Singh A, Gaur R. Comparative analysis and applications of green synthesized cobalt oxide (Co3O4) nanoparticles: a systematic review. BioNanoScience. 2024;14:3536-3554.
16. Govindasamy K, Senthilkumar S, Ganesh T. Eco-friendly synthesis of Co3O4 nanoparticles using Ipomoea staphylina leaf extract: photocatalytic, antibacterial, and antioxidant properties. ChemistrySelect. 2025;10:e03074.
17. Umar HM, Zangina T, Sumaila JL, Dwivedi A, Aamir M. Green synthesis of silver and zinc oxide nanoparticles using Ziziphus jujuba: mechanisms, characterization, applications, and future perspectives. J Mater Sci Mater Energy. 2026;2:9.
18. Jadhav NV, Pore DM, Patre BK. Role of Moringa oleifera on green synthesis of metal/metal oxide nanomaterials. J Nanomater. 2022;2022:2147393.
19. Leone A, Spada A, Battezzati A, Schiraldi A, Sironi J, Akoh CC, et al. Moringa oleifera seeds and oil: characteristics and uses for human health. Int J Mol Sci. 2016;17(12):2141.
20. Dwivedi A, Umar HM, Ahmed G, Vaswani J, Varshney P. Enhanced structural and magnetic properties of ABS5 compared to AAS5 and ACS5: a combined XRD, SEM, and VSM study. SSRG Int J Mater Sci Eng. 2026;12(2):1-9.
21. Mohanpuria P, Rana NK, Yadav SK. Biosynthesis of nanoparticles: technological concepts and future applications. J Nanoparticle Res. 2008;10:507-517.
22. Raimundo RA, Lourenço CS, Câmara NT, Silva TR, Santos JRD, Araújo AJM, et al. Green synthesis of Co3O4 nanoparticles using psyllium husk (Plantago ovata) and application as electrocatalyst for oxygen evolution reaction. J Electroanal Chem. 2023;934:117218.
23. Goldstein JI, Newbury DE, Michael JR, Ritchie NWM, Scott JHJ, Joy DC. Scanning electron microscopy and X-ray microanalysis. 4th ed. New York: Springer; 2018.
24. Williamson GK, Hall WH. X-ray line broadening from filed aluminium and wolfram. Acta Metall. 1953;1(1):22-31.
25. Lee YS, Ryu H, Shin GH, Jeong ED, Bai CJ. Synthesis and properties of cobalt oxide nanoparticles. Trans Electr Electron Mater. 2014;15(5):249-252.
26. Rana A, Yadav K, Jagadevan S. A comprehensive review on green synthesis of nature-inspired metal nanoparticles: mechanism, application and toxicity. J Clean Prod. 2020;272:122880.
27. Jadoun S, Arif R, Jangid NK, Meena RK. Green synthesis of nanoparticles using plant extracts: a review. Environ Chem Lett. 2021;19:355-374.
28. Newbury DE, Ritchie NWM. Performing elemental microanalysis with high accuracy and high precision by scanning electron microscopy/silicon drift detector energy-dispersive X-ray spectrometry. J Mater Sci. 2015;50:493-518.
29. Ndepete CP, Sinha S. Band gap determination for Co3O4 nanoparticles synthesized using Moringa oleifera and their photocatalytic properties. Opt Mater. 2021;112:110731.
30. Sun H, Ang HM, Tadé MO, Wang S. Co3O4 nanocrystals with predominantly exposed facets: synthesis, environmental and energy applications. J Mater Chem A. 2013;1(46):14427-14442.
31. Annu, Sahu M, Singh S, Prajapati S, Verma DK, Shin DK. From green chemistry to biomedicine: the sustainable symphony of cobalt oxide nanoparticles. RSC Adv. 2024;14:32733-32758.

32. Yan W, Huang L, Xu X, Deng Z, Yang W, Xu J. Co3O4 nanocubes for highly sensitive gas sensing. Sens Actuators B Chem. 2022;364:131862.
33. Ahmad I, Umar A, Ibrahim AA, Kumar R, Algarni H, Choudhary MK. Fabrication, characterization and photocatalytic application of Co3O4/ZnO nanocomposites. Ceram Int. 2024;50:3462-3471.
34. AlSalhi MS, Oza G, Castillo-Maldonado I, Sharma A. Evaluation of antimicrobial, antioxidant, and anti-inflammatory abilities of sustainably synthesized Co3O4 NPs. Biocatal Agric Biotechnol. 2024;56:103025.
35. Elazem NYA, Mubarak M, El-Mossalamy EH. Enhancing pseudocapacitive properties of cobalt oxide hierarchical nanostructures via iron doping. Heliyon. 2023;9(4):e14503.
36. Yuan C, Yang L, Hou L, Shen L, Zhang X, Lou XW. Growth of ultrathin mesoporous Co3O4 nanosheet arrays on Ni foam for high-performance electrochemical capacitors. Energy Environ Sci. 2012;5:7883-7887.
37. Leninbarathi K, Bharath G, Sathiyaraj S, Ranjith Kumar E, Srinivas C, Hegde VN, et al. Green synthesized of Co3O4 nanoparticles and their structural, optical, elastic, morphological and colloidal stability. Int Res J Multidiscip Technovation. 2026;8:1-15.
38. Saleh HA, Umar HM, Adam A, et al. Recent advances in neem-mediated green synthesis of Ag-doped ZnO nanostructures: fundamentals, characterization, visible-light photocatalysis, and optoelectronic applications. J Mater Sci Mater Eng. 2026.
39. Umar HM, Sumaila JL, Zangina T. Comparative structural, optical, morphological and elemental characterization of jujube-mediated silver and zinc oxide nanoparticles. FUDMA J Sci. 2026;10(19):219-229.